Biomolecular NMR Assignments (2026) 20:8
https://doi.org/10.1007/s12104-025-10251-4

ARTICLE

Backbone NMR resonance assignments for the C2 domain of the *Streptococcus mutans* adhesin P1

Emily-Qingqing Peng[1] · M. Luiza Caldas Nogueira[1,2] · Chase Norton[1] · L. Jeannine Brady[3] · Joanna R. Long[1,2]

Received: 24 July 2025 / Accepted: 13 October 2025

Abstract

Adhesin P1 (aka AgI/II) is an extracellular protein regulating adherence and detachment of *Streptococcus mutans* in the oral cavity and thus plays a pivotal role in biofilm development and maturation. P1's naturally occurring C-terminal truncation product, Antigen II (AgII), adopts both soluble, monomeric and insoluble, amyloidogenic forms during the bacterial life cycle. Monomeric AgII forms important quaternary interactions with P1's A3VP1 segment that is projected from the bacterial cell surface to promote cell adhesion, while the functional amyloid form of AgII promotes detachment of mature biofilms. The heterologous recombinant 51-kD C123 construct, comprising most of AgII, has been characterized by X-ray crystallography and serves as a functional surrogate of AgII in studies of adhesion and biofilm regulation. C123 contains three structurally similar domains, C1, C2, and C3. Using Alphafold prediction and the C123 crystal structure, we identified domain boundaries within C123 to develop more tractable constructs for NMR studies, including quaternary interactions with other proteins. The C2 domain is of particular interest because it contains several unique helices in addition to the β-sheet fold it shares with the C1 and C3 domains. Here we report the backbone NMR resonance assignments for the C2 construct. Secondary structure predictions from NMR assignments are in good agreement with those anticipated by Alphafold and the observed crystal structure, except for some of the helices suggesting they are more dynamic. We then compare C2 chemical shift perturbations caused by quaternary interactions with recombinant A3VP1, as well as by a monoclonal antibody, MAb 6–8C, known to inhibit bacterial adherence and C123 binding to A3VP1. We note the C2 chemical shift perturbations are markedly different from previously observed interactions of C3 with A3VP1 and MAb 6–8C, providing further insight on how the individual domains of C123 may vary in their ability to mediate bacterial adhesion and formation of functional amyloid. The prior NMR assignment and characterization of C3 combined with the NMR assignment and characterization of C2 described here provide a foundation for further NMR studies, including assignment of C23 and C123 constructs, protein-protein interaction studies of C23 and C123, assessing the impact of environmental conditions on structure and dynamics within C123 as it transitions from monomer to amyloid form, and the functional relevance of having three successive domains with similar tertiary folds.

Keywords *Streptococcus mutans* adhesin P1 · C2 domain · NMR · Quaternary interaction

Abbreviations

CSI	Chemical Shift Index
Δδ	Chemical shift perturbation (CSP)

Biological context

Streptococcus mutans (*S. mutans*) is a gram-positive bacterium commonly associated with dental caries, one of the most prevalent human diseases in the world (Lemos et al. 2019). The cell surface-localized protein adhesin called P1

✉ Joanna R. Long
jrlong@ufl.edu

[1] Department of Biochemistry and Molecular Biology and McKnight Brain Institute, University of Florida, Gainesville, FL 32610-0245, USA

[2] National High Magnetic Field Laboratory, University of Florida, Gainesville, FL 32610-0245, USA

[3] College of Dentistry, Department of Oral Biology, University of Florida, Gainesville, FL 32610, USA

Published online: 13 December 2025

(aka Antigen I/II, AgI/II) mediates sucrose-independent *S. mutans* adhesion, which facilitates bacterial colonization and biofilm formation on the tooth surface (Russell et al. 1980; Brady et al. 2010; Abranches et al. 2018). P1's C-terminus includes three tandem globular domains (C123) upstream of the LPxTG consensus motif recognized by the transpeptidase Sortase A for attachment of P1 to the peptidoglycan matrix. AgII is a naturally occurring C-terminal truncation product of P1. Cell wall attached, full-length P1 is inaccessible to several monoclonal antibodies (MAbs) whose epitopes lie within the AgII segment, but the extracellular AgII derivative is readily detectable within culture supernatants and is recognized by these antibodies (Heim et al. 2015). Extracellular AgII contributes to the adhesive properties of cell wall-attached P1 via its quaternary interactions with P1's globular head which is projected outward from the cell wall by a hybrid stalk comprised of intertwined α- and polyproline helices (Larson et al. 2010; Heim et al. 2015). We utilize a recombinant C123 polypeptide as a surrogate for AgII in our in vitro experiments and a recombinant A3VP1 polypeptide as a surrogate for the projected adhesin. Upon mechanical stirring, both C123 and full-length P1 form insoluble aggregates that exhibit classic amyloid properties (Oli et al. 2012; Besingi et al. 2017; Barran-Berdon et al. 2020). Recently we demonstrated that *S. mutans* amyloid aggregates are localized to the non-adherent fraction of aging biofilms, and that amyloid formation diminishes *S. mutans* adhesion (Yarmola et al. 2022). Thus, the C-terminal derivative of P1 plays a major regulatory role not only in initial adhesion and biofilm genesis through quaternary interactions of its monomeric form with other P1 domains, but also in biofilm maturation and detachment through the formation of functional amyloid. Identifying environmental cues that trigger the conversion of AgII from monomeric to amyloid form are the subject of ongoing research.

In our initial structural studies of recombinant C123, this heterologously expressed construct was crystallized and found to contain three structurally similar domains, C1, C2, and C3 (Larson et al. 2011). Each domain exhibited a DE-variant IgG-fold whose β-sheet structure was stabilized by an intramolecular isopeptide bond. Individually cloned and expressed C1, C2, and C3 constructs were also characterized. In order to use NMR to evaluate C123 quaternary interactions with other segments of P1, and possible structural changes consequent to such interaction, we started with the assignment of a C3 construct, since the complete C123 construct was >50 kD and prone to aggregation (Rivière et al. 2019). We were able to assign ~60% of the residues within C3 and confirmed via chemical shift analysis that its secondary structure was consistent with the available C123 crystal structure (BMRB Entry 27935). Importantly, we were also able to map C3's interactions with P1's A3VP1 and C12 segments as well as with a MAb 6–8C, which binds to C123. Despite its tractable 17 kD size and high stability in solution, we were unsuccessful in finding NMR conditions that enabled full assignment of this original C3 construct.

The original C123 construct was designed to enhance the likelihood of crystallization. The resulting structural model (1) identified likely boundaries of the individual C1, C2, and C3 domains, and (2) eliminated the C-terminal cell wall and membrane-spanning segments of intact P1 including the LPxTG sortase motif, which are predicted to be unstructured. To further our NMR studies, we recently reanalyzed the likely domain boundaries within C123 using AlphaFold 2.0. This analysis revealed that P1's C3 domain is predicted to contain an additional seven amino acids compared to the original C3 and C123 constructs. These additional residues extend the β-sheet structure at C3's C-terminus and increase its structural homology with C1 and C2. Using a new construct for C3 containing these seven residues, we assigned 92% of the C3 backbone amide resonances (Peng et al. 2023), confirmed binding interactions with A3VP1 and MAb 6–8C that were consistent with our prior work, and more clearly identified the binding interfaces with these proteins (Tang et al. 2016).

We report herein the backbone (^{13}Cα, ^{13}Cβ, ^{13}CO, ^{15}NH, ^{1}HN, ^{1}Hα, and ^{1}Hβ) assignments for a new C2 construct made based on our AlphaFold analysis. We were able to assign 91% of the protein backbone amide resonances. We note that the C2 domain, while possessing a similar β-sheet fold to C3, contains several small helices based on the C123 crystal structure and Alphafold predictions for the C2 domain in isolation. The NMR data we report here suggest these helices are structurally labile, providing a possible nucleus for induction of functional amyloid formation. We also characterize the interactions of C2 with A3VP1 and MAb 6–8C. Both these proteins cause chemical shift perturbations, but their interactions with C2 are markedly different relative to their interactions with C3.

Studying both the C2 and C3 domains provides valuable insights into their individual structural and functional properties, including their unique interactions with other proteins. Both domains are predominantly β-sheet in their secondary structures and interact with the monoclonal antibody MAb 6–8C, highlighting their shared features. However, C2 contains additional α-helices and C3 exhibits a stronger interaction with A3VP1, indicating distinct functional properties. While C2 and C3 are individually stable in solution and remain as monomers for extended periods, the C23 and C123 constructs display significant amyloidogenic properties. This suggests that the amyloidogenic nature of C23 arises from the combined presence of both domains rather than from a single domain alone. C3 is notably non-amyloidogenic in isolation; it also interacts with C12 to

recapitulate the C2/C3 domain interfact observed within C123. Mixing of C3 with C12 did not lead to any observable amyloid formation, although this was not extensively tested under either stirring or variable pH conditions. Identifying the dynamic nature of the helices in C2 provides potential starting points for monitoring the conversion of C23 and C123 from monomer to amyloid. This new information also provides a more complete mechanistic understanding of how 6–8C interferes with AgII's interaction with cell-associated P1, thereby enabling it to inhibit *S. mutans* adhesion to its physiologic substrate in saliva (Heim et al. 2014). Our new data will also enable the assignment of C23 and C123 constructs as we track structural changes within P1 and AgII in response to environmental triggers such as pH, bivalent cations, or quaternary interactions with other biomolecules.

Methods and experiments

Protein expression and purification

The DNA sequence coding for the C2 domain of adhesin P1 (residues 1155–1328; Uniprot accession number P23504) was synthesized, with codon optimization for *E. coli*, by Genescript and inserted into pET21a(+) plasmid to yield the pET21a-C2-His_6 plasmid with a C-terminal His tag. The pET21a-C2-His_6 plasmid was transformed into *E. coli* BL21(DE3) cells for overexpression. A single colony was grown in 5 mL of terrific broth supplemented with 100 µg/mL ampicillin at 37 °C overnight. This pre-culture was added to 1 L of an optimized M9 minimal medium containing 2.7 g/L $^{15}NH_4Cl$, 4 g/L $^{13}C_6$-D-glucose, 7.1 g/L Na_2HPO_4, 6.8 g/L KH_2PO_4, and 0.7 g/L Na_2SO_4 with 100 µg/mL ampicillin. Cells were grown at 37 °C to an OD_{600} of ~0.8. The incubation temperature was then reduced to 30 °C and protein expression was induced by addition of 1 mM isopropyl-β-D-thiogalactopyranoside (IPTG). After 16 h at 30 °C, the cells were pelleted by centrifugation at 6,000 x g at 4 °C for 30 min. The cells were resuspended in 40 mL of lysis/binding buffer (30 mM Tris pH 7.4 containing 100 mM NaCl, 20 mM Imidazole and 1 mM PMSF). Resuspended cells were frozen, thawed, sonicated, and cellular debris was removed via centrifugation at 39,000 x g for 90 min at 4 °C. The supernatant containing recombinant C2 was filtered using a 0.45 µm syringe filter and loaded onto a 5 mL HisTrap-HP column (Cytiva). The column was washed with 10 column volumes of lysis/binding buffer. C2 was eluted from the column with 10 volumes of elution buffer (30 mM Tris pH 7.4 containing 100 mM NaCl, 300 mM Imidazole and 1 mM PMSF). The elution fractions were analyzed by SDS-PAGE with Coomassie staining and protein purity was verified by observation of a single intense band at the expected molecular weight. Fractions containing protein were combined and dialyzed against 50 mM phosphate buffer pH 8 containing 100 mM NaCl at 4 °C overnight. The dialyzed supernatant was concentrated using a 10 kDa MWCO centrifugal concentrator (Amicon Ultra-15 10 K). Prior to NMR experiments, samples were exchanged into NMR buffer (50 mM sodium phosphate, 50 mM NaCl, 10% (v/v) D_2O, 1 mM sodium trimethylsilyl proprionate (TSP) at pH 6.5).

NMR spectroscopy

NMR experiments for backbone assignments were recorded at 298 K, using an 800 MHz Bruker spectrometer (Avance II) equipped with a TCI cryoprobe and a 440 µM sample of ^{15}N,^{13}C-enriched C2. Backbone assignments were obtained from 3D experiments using Bruker pulse sequences for BEST-HNCO, -HN(CA)CO, -HNCA, -HN(CO)CA, -HNCACB, -HN(CO)CACB, and standard HBHA(CO)NH correlations (Table 1). The data were acquired and processed using Topspin 3.7.0 (Bruker Biospin). TSP was used as the ^1H chemical shift reference, and the ^{15}N and ^{13}C chemical shifts were indirectly referenced based on ^1H chemical shifts. The NMR data were analyzed using CcpNmr Analysis V3 (Vranken et al. 2005).

Chemical shift perturbation measurements

Protein-protein interaction surfaces on uniformly ^{15}N-enriched C2 were characterized by CSPs measured using ^{1}-^{15} N-TROSY experiments recorded with a fixed

Table 1 List of NMR experiments acquired at 800 MHz and corresponding parameters used for C2 assignment

Experiment	Time domain size (pts)			Spectral width/Carrier Frequency (ppm)			Delay
	T1	T2	T3	F1	F2	F3	
^{15}N TROSY	2048	256		15/4.7	36/120	-	0.2 s
HN(CO)CACB	2048	64	128	15/4.7	36/120	64/42.6	0.2
HNCACB	2048	64	128	15/4.7	36/120	64/42.6	0.2
HNCO	2048	64	48	15/4.7	36/120	12/173	0.2
HN(CA)CO	2048	64	48	15/4.7	36/120	12/173	0.2
HN(CO)CA	2048	64	80	15/4.7	36/120	40/45.85	0.2
HNCA	2048	64	128	15/4.7	36/120	40/45.85	0.2
HBHA(CO)NH	2048	64	128	15/4.7	36/120	10/4.7	1

molar ratio of ligand candidates: A3VP1 (protein ratio 1:1 C2:A3VP1) or MAb 6–8C (protein ratio ~ 30:1 C2:MAb 6–8C). Samples contained 50 µM ^{15}N-enriched C2 in NMR buffer. The spectral perturbations were quantified as the combined amide CSPs, specifically for each amide resonance the CSP was calculated as:

$$\Delta\delta = \sqrt{(\Delta\delta_H)^2 + (\Delta\delta_N/5)^2}$$

Where $\Delta\delta_H$ and $\Delta\delta_N$ are the change in chemical shift for an amide resonance in the ^{1}H and ^{15}N dimensions, respectively. The change in ^{15}N chemical shift is scaled down five-fold in calculating the combined CSP to reflect the different chemical shift ranges observed for the ^{15}N resonances (~25 ppm) compared to the ^{1}H resonances (~5 ppm).

Extent of assignment and data deposition

The 2D ^{1}H, ^{15}N TROSY spectrum of the C2 domain (residues 1155-1328 of the full-length adhesin P1 protein, Uniprot accession number P23504) displays well-dispersed resonances with minimal overlap (Fig. 1a). Sequence-specific resonance assignments for 152 of 167 possible C2 ^1H_N-^{15}N correlations (91%) were unambiguously determined using heteronuclear multidimensional NMR methods (Fig. 1a). Using these 152 correlations, 161 ^{13}Cα resonances (93%), 138 ^{13}Cβ resonances (87%), 160 ^{13}CO resonances (92%), and 125 ^{1}Hα resonances (72%) were assigned. Unassigned residues are primarily within two β-sheet regions (Fig. 1b). In order to verify the secondary structural elements of C2, the chemical shift assignments of backbone atoms (HN, Hα, Cα, Cβ, CO, and N) were analyzed with the CSI 3.0 (Hafsa et al. 2015). The returned secondary structure predictions were aligned with a predicted structure from AlphaFold3 and the C2 domain from the C123 crystal structure (Fig. 2a). Overall, there is good agreement between these three methods. The primary difference for the NMR data is a slightly lower helical content. Compared to the C3 domain, C2 maintains a similar β-sheet fold but contains additional helices (Fig. 1c; (Larson et al. 2011; Peng et al. 2023). The lower helical content for the NMR data compared to the X-ray data suggest these helices may be more dynamic in solution and are stabilized by crystal-packing interactions. This is supported by the AlphaFold3 prediction also having lower helical content albeit intermediate between the NMR and X-ray data (Fig. 2b). These helices represent regions that may provide the plasticity needed for the C23 and C123 proteins to convert from soluble monomers to an extended β-sheet that is the hallmark of amyloid formation. While we did not remove the C-terminal His6 tag from the construct prior to NMR measurements, it was too dynamic to assign and is unlikely to contribute to the improved resolution and observed structure.

Interactions of C2 with MAb 6–8C and A3VP1

Binding to MAb 6–8C induces significant CSPs for several residues within C2 (Fig. 3a). Mapping these perturbations on to the Alphafold predicted structure of C2 shows that some of the perturbed residues encompass a region predicted to be helical but whose backbone chemical shifts

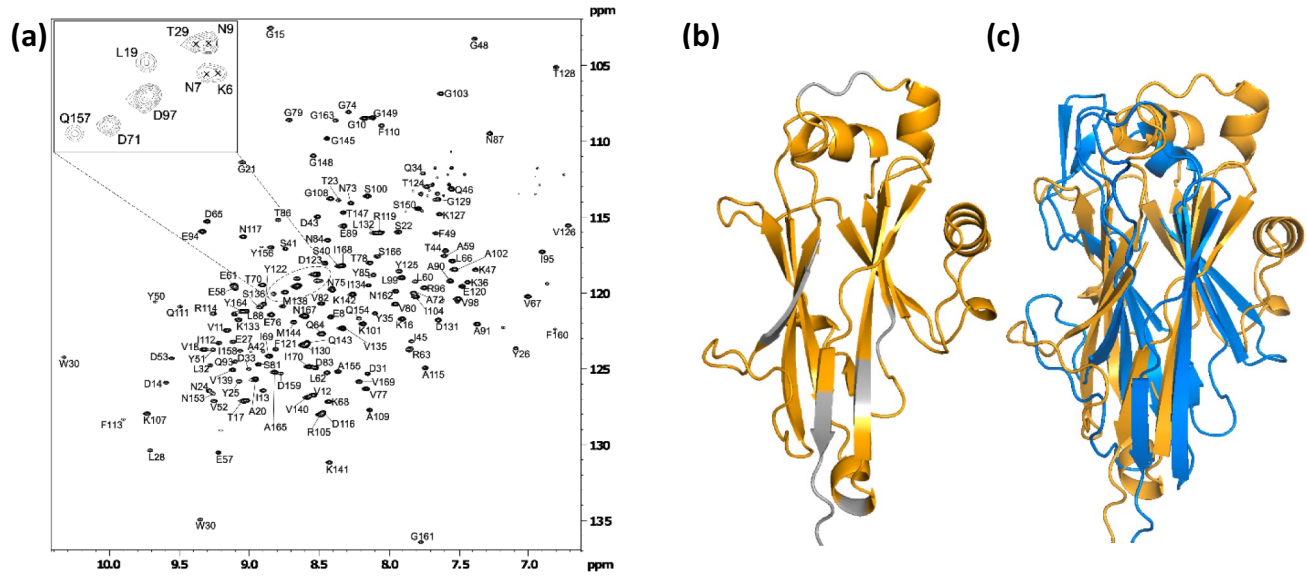

Fig. 1 (**a**) Annotated 2D ^{1}H,^{15}N BEST-TROSY spectrum for Adhesin P1 C2 domain (BMRB 52909) collected at 800 MHz and 25 °C in phosphate buffer, pH 6.5. Resonance assignments are labelled in black; (**b**) AlphaFold3 structural model for the C2 construct with the NMR-assigned amino acid residues shown in orange; (**c**) Overlay of AlphaFold3 predicted structures for C2 (orange) and C3 (blue) domains

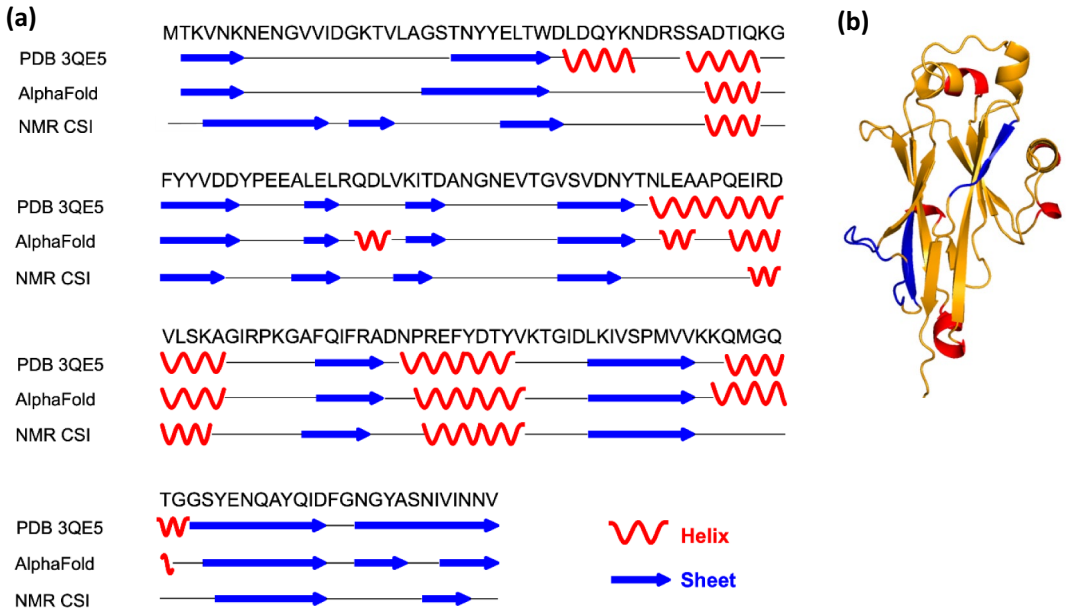

Fig. 2 (**a**) Comparison of observed and predicted secondary structures for the C2 domain. Shown are alignments of the observed secondary structure for the C2 domain within the X-ray structure of the C123 construct (PDB 3QE5), the predicted secondary structure (using AlphaFold3) for the C2 domain in isolation, and the predicted secondary structure based on C2 chemical shifts (using CSI 3.0) for the C2 construct in the present study (BMRB 52909); (**b**) AlphaFold3 predicted structure for C2 highlighting differences in secondary structure for helices (red) and sheets (blue) compared to CSI 3.0 secondary structure prediction based on the observed chemical shifts

suggest less helical content (Fig. 3b). Binding of C2 to A3VP1 also induced CSPs (Fig. 3c). A notably different pattern was observed upon interaction of C2 with A3VP1 in comparison to its interaction with MAb 6–8C. The magnitude of the CSPs were also significantly lower for A3VP1 addition even though A3VP1 and C2 were mixed at a 1:1 ratio while MAb 6–8C and C2 were mixed at a 1:30 ratio. The CSPs for C2 upon A3VP1 binding are primarily located in loop regions (Fig. 3d), while the strongest CSPs localized to different regions of C2 upon MAb 6–8C binding.

Comparisons of C2 and C3 interactions with MAb 6–8C and A3VP1

The CSPs for C2 interacting with MAb 6–8C indicate that, as previously reported for C3, there are well-defined binding interactions, leading to strong localized CSPs with some resonances reaching $\Delta\delta$ values >0.1 ppm even when the MAb concentration is much lower than the C2 or C3 concentration. We note that for our 2023 study, we performed CSP experiments for C3 using unpurified MAb 6–8C in ascites fluid at a reported ratio of 6:1, whereas in the current study we employed purified 6–8C at much lower ratio. In ascites, the concentration of functional antibody is much lower than the apparent total protein concentration, while in the freshly purified MAb preparation there is a direct correspondence of protein concentration and functional MAb. For the present study, we repeated the experiment for C3 interacting with MAb 6–8C using purified antibody at a ratio of 50:1 and confirmed the CSPs observed in our prior study were observed at a much lower protein ratio when working with purified antibody. When the largest CSPs are mapped on to the protein sequences and structures (Fig. 4), it appears MAb 6–8C may recognize the shared tertiary fold of C2 and C3 rather than specific loop/helical regions of either protein. There is a shared β-sheet rich domain between C2 and C3, but differences in sequence and loop/helical regions apparently lead to the observed differences in MAb 6–8C's binding interfaces with C2 compared to C3.

In the case of A3VP1, there is an even more notable difference in binding to C2 vs. C3. The CSP magnitudes on addition of A3VP1 at a 1:1 ratio are as high as 0.21 ppm in C3 compared to <0.07 ppm at equimolar concentrations of A3VP1 and C2 or C3. While some of this variability can be attributed to differences in the C2 concentration (50 μM) vs. the C3 concentration (130 μM) for these experiments, it also suggests that A3VP1 may bind more strongly and may have a higher affinity for the C3 domain compared to the C2 domain. Unlike what we observed for the C3 domain (Peng et al. 2023), where A3VP1 and MAb 6–8C CSPs demonstrated considerable overlap in their binding sites, the interaction of C2 with A3VP1 is markedly weaker compared to MAb 6–8C and no overlap was observed between the A3VP1 and MAb 6–8C binding sites. These results suggest that sequence differences in C2 vs. C3 and loop/helical regions govern their respective abilities to bind A3VP1

w

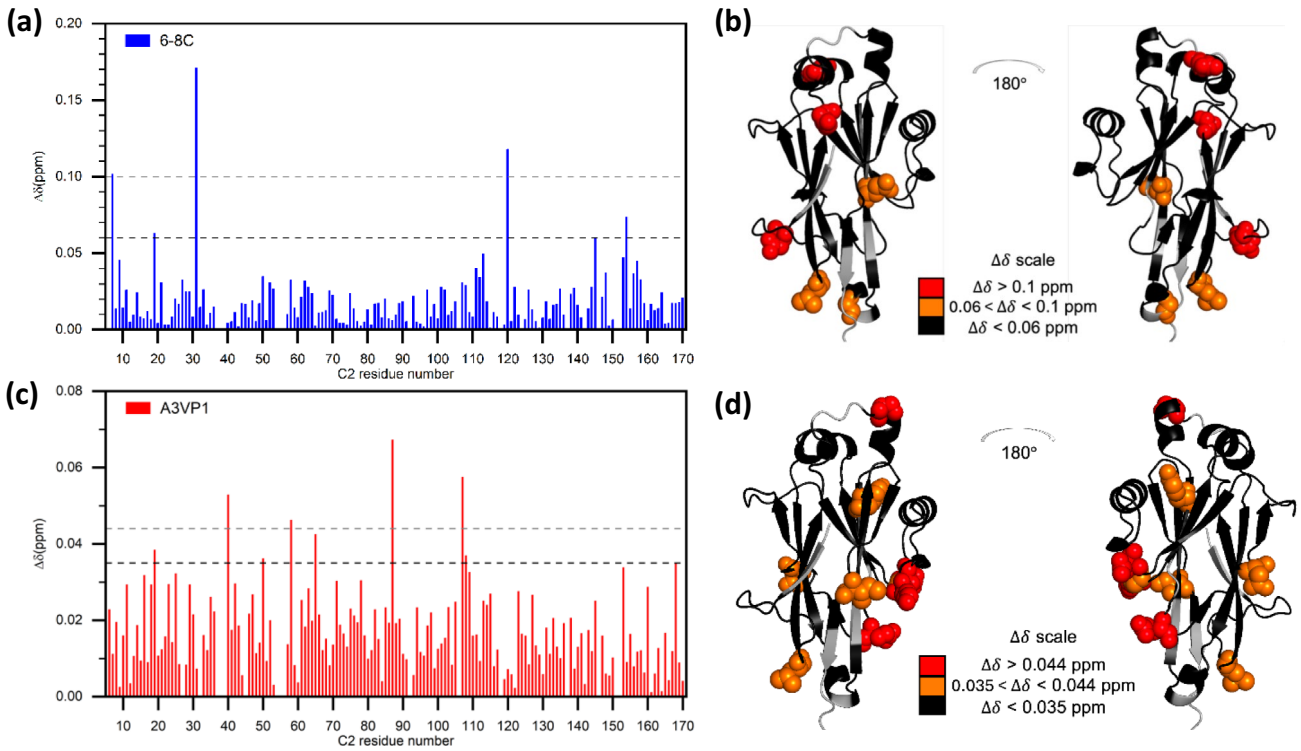

Fig. 3 Mapping of MAb 6–8C and A3VP1 interactions with the C2 domain construct. (**a**) Δδ for specific C2 amide resonances upon addition of MAb 6–8C (protein ratio ~ 30:1 C2:6–8C). Dashed lines indicate perturbations greater than two or four standard deviations. (**b**) C2 residues perturbed by more than two standard deviations on 6–8C binding mapped onto the C2 structure predicted by AlphaFold3. (**c**) Δδ for specific C2 amide resonances upon addition of A3VP1 (protein ratio 1:1) at pH 6.5. Dashed lines indicate perturbations greater than two or three standard deviations. (**d**) C2 residues perturbed by more than two standard deviations on A3VP1 binding mapped onto the C2 structure predicted by AlphaFold3

compared to MAb 6–8C. Most notably, the three-amino acid sequence HSE that precedes the 4th β-sheet in C3 was identified as important for binding of both A3VP1 and MAb 6–8C. The corresponding sequence in C2 is YPE, and it is located right after its 4th β-sheet.

Given that C3 has a stronger interaction with A3VP1 than C2, it is likely the primary site for monomeric AgII (C123) to interact with intact P1 on the *S. mutans* cell wall surface to enhance cellular adhesion (Heim et al. 2015). However, C3 is insufficient for a monomeric polypeptide to transition to an amyloid form. It is the amyloid form of AgII (C123) that correlates with biofilm detachment (Yarmola et al. 2022), in contrast to the monomeric form that correlates with bacterial adhesion (Heim et al. 2015).We speculate therefore that during biofilm progression of aging cultures that amyloid aggregation is facilitated by as yet unknown environmental factors to quench the adhesive activity of the P1-AgII quaternary complex (di Cologna et al. 2021; Yarmola et al. 2022). Since C3 alone is insufficient to mediate amyloid formation, but the presence of C2 enables aggregates to form, it is likely that nuances in the interactions of individual domains of C123 with other proteins and with itself are critical determinants of biofilm progression from initial attachment to detachment. As documented by this study, C2 has a weaker interaction with A3VP1 and has regions that are helical in its crystalline form that become more disordered in solution as measured by NMR chemical shifts. We are currently pursuing NMR experiments to structurally characterize C23 and C123 constructs as well as environmental triggers of dynamics or structural transitions. The observation of structurally labile, short helices provides guidance for specific residues that can be isotopically enriched for querying changes in C123 structure via lower resolution solid-state NMR measurements within the context of intact cell walls and/or functional amyloid formation (Tang et al. 2016).

Fig. 4 Comparison of C2 and C3 interactions with (**a**) MAb 6-8C and (**b**) A3VP1. (**a**) C2 and C3 interactions with MAb 6-8C based on CSPs. Residues are color-coded based on the magnitude of CSPs at a 1:>30 ratio of purified MAb 6-8C to C2 or C3. Red indicates the largest perturbations (≥ 0.1) while orange indicates moderately strong perturbations (≥0.05). Residues with smaller CSPs are shown in black. C2 and C3 structures predicted by AlphaFold3; MAb model based on PDB 5DK3, an IgG4 antibody. (**b**) C2 and C3 interactions with A3VP1 based on CSPs upon interaction with A3VP1 at a 1:1 ratio. Residues are colorcoded based on the magnitude of CSPs: red indicates the largest perturbations (≥ mean + 6SD or 0.4 ppm for C3) while orange indicates moderately strong perturbations (≥ mean + 3SD or 0.04 and 0.25 ppm for C2 and C3, respectively). Residues with CSPs below mean+3SD are shown in black. C2 and C3 structures predicted by AlphaFold3; A3VP1 model based on PDB 3IOX. C3 interactions are from prior work (Peng et al. 2023).

Acknowledgements We thank James Collins and James Rocca for technical assistance with NMR experiments.

Author contributions E.Q.P. performed protein expression and purification, collected the NMR data, analyzed the data and wrote the first draft of the manuscript. M.L.C.N. assisted with plasmid design, NMR data collection, and analysis. C.N. assisted with protein expression and purification. All authors commented on previous versions of the manuscript and reviewed the final submitted manuscript. Funding acquisition and supervision were done by L.J.B. and J.R.L.

Funding This work was supported by NIH/NIDCR R01/R56 DE021789 to L.J.B. and J.R.L. A portion of this work was performed in the McKnight Brain Institute at the National High Magnetic Field Laboratory's AMRIS Facility, which is supported by National Science Foundation Cooperative Agreement DMR-2128556, the State of Florida, and an NIH award, S10 OD028753, for magnetic resonance instrumentation.

Data availability The chemical shift values for P1 Adhesin C2 domain were deposited in the Biological Magnetic Resonance Data Bank (BMRB) under accession code 52909.

Declarations

Competing interests The authors declare that they have no conflict of interest.

Ethics approval and consent to participate Not applicable.

Consent for publication All the authors have seen and approved the submission of this manuscript.

References

Abranches J, Zeng L, Kajfasz JK et al (2018) Biology of oral Streptococci. Microbiol Spectr 6:5–6

Barran-Berdon AL, Ocampo S, Haider M et al (2020) Enhanced purification coupled with biophysical analyses shows cross-β structure as a core Building block for Streptococcus mutans functional amyloids. Sci Rep 10:1–11

Besingi RN, Wenderska IB, Senadheera DB et al (2017) Functional amyloids in *Streptococcus mutans*, their use as targets of biofilm inhibition and initial characterization of SMU_63c. Microbiology 163:488–501. https://doi.org/10.1099/mic.0.000443

Brady LJ, Maddocks SE, Larson MR (2010) The changing faces of Streptococcus antigen I/II polypeptide family adhesins. Mol Microbiol 77:276–286

di Cologna NM, Samaddar S, Valle CA et al (2021) Amyloid aggregation of Streptococcus mutans Cnm influences its collagen-binding activity. Appl Environ Microbiol 87:e01149–e01121

Hafsa NE, Arndt D, Wishart DS (2015) CSI 3.0: a web server for identifying secondary and super-secondary structure in proteins using NMR chemical shifts. Nucleic Acids Res 43:W370–W377

Heim KP, Crowley PJ, Long JR et al (2014) An intramolecular lock facilitates folding and stabilizes the tertiary structure of Streptococcus mutans adhesin p1. Proc Natl Acad Sci U S A 111:15711–15716. https://doi.org/10.1073/pnas.1413018111

Heim KP, Sullan RMA, Crowley PJ et al (2015) Identification of a supramolecular functional architecture of Streptococcus mutans adhesin P1 on the bacterial cell. J Biol Chem 290:9002–9019. https://doi.org/10.1074/jbc.M114.626663

Larson MR, Rajashankar KR, Patel MH et al (2010) Elongated fibrillar structure of a streptococcal adhesin assembled by the high-affinity association of α-and PPII-helices. Proc Natl Acad Sci U S A 107:5983–5988

Larson MR, Rajashankar KR, Crowley PJ et al (2011) Crystal structure of the C-terminal region of Streptococcus mutans antigen I/II and characterization of salivary agglutinin adherence domains. J Biol Chem 286:21657–21666. https://doi.org/10.1074/jbc.M111.231100

Lemos JA, Palmer SR, Zeng L et al (2019) The biology of Streptococcus mutans. Microbiol Spectr 7(1). https://doi.org/10.1128/microbiolspecGPP3-0051-2018

Oli MW, Otoo HN, Crowley PJ (2012) Functional amyloid formation by *Streptococcus mutans*. Microbiology 158:2903

Peng E-Q, Caldas Nogueira ML, Rivière G (2023) Backbone NMR resonance assignments for the C terminal domain of the Streptococcus mutans adhesin P1. Biomol NMR Assign 17:293–299

Rivière G, Peng EQ, Brotgandel A (2020) Characterization of an intermolecular quaternary interaction between discrete segments of the *Streptococcus mutans* adhesin P1 by NMR spectroscopy. FEBS J. https://doi.org/10.1111/febs.15158

Russell MW, Bergmeier LA, Zanders ED, Lehner T (1980) Protein antigens of *Streptococcus mutans*: purification and properties of a double antigen and its protease-resistant component. Infect Immun 28:486–493

Tang W, Bhatt A, Smith AN et al (2016) Specific binding of a naturally occurring amyloidogenic fragment of *Streptococcus mutans* adhesin P1 to intact P1 on the cell surface characterized by solid state NMR spectroscopy. J Biomol NMR 64:153–164

Vranken WF, Boucher W, Stevens TJ (2005) The CCPN data model for NMR spectroscopy: development of a software pipeline. Proteins 59:687–696

Yarmola E, Ishkov IP, di Cologna NM et al (2022) Amyloid aggregates are localized to the nonadherent detached fraction of aging Streptococcus mutans biofilms. Microbiol Spectr 10:e01661–e01622